ACS APPLIED MATERIALS & INTERFACES

Research Article

Cite This: ACS Appl. Mater. Interfaces 2018, 10, 31648−31654

www.acsami.org

Reversible Tuning of the Ferromagnetic Behavior in Mn-Doped MoS_2 Nanosheets via Interface Charge Transfer

Hao Tan,[†] Chao Wang,[‡] Wei Hu,[†] Hengli Duan,[†] Peng Guo,[†] Na Li,[†] Guinan Li,[†] Liang Cai,[†] Zhihu Sun,*[,†] Fengchun Hu,[†] and Wensheng Yan*[,†]

[†]National Synchrotron Radiation Laboratory, University of Science and Technology of China, Hefei 230029, P. R. China

[‡]Key Laboratory of Neutronics and Radiation Safety, Institute of Nuclear Energy Safety Technology, Chinese Academy of Sciences, Hefei 230031, Anhui, P. R. China

Supporting Information

ABSTRACT: Reversible manipulation of the magnetic behavior of two-dimensional van der Waals crystals is crucial for expanding their applications in spin-based information-processing technologies. However, to date, most experimental approaches to tune the magnetic properties are single way and have very limited practical applications. Here, we report an interface charge-transfer method for obtaining a reversible and air-stable magnetic response at room temperature in Mn-doped MoS_2 nanosheets. By adsorption of benzyl viologen (BV) molecules as the charge donor, the saturation magnetization of Mn-doped MoS_2 nanosheets is enhanced by a magnitude of 60%, and the magnetization can be restored to the original value when the adsorbed BV molecules are removed. This cycle can be repeated many times on the same sample without detectable degradation. Experimental characterizations and first-principles calculations suggest that the enhanced magnetization can be attributed to the increase of Mn magnetic moment because of the enriched electrons transferred from BV molecules. This work shows that interface charge transfer may open up a new pathway for reversibly tuning the exchange interactions in two-dimensional nanostructures.

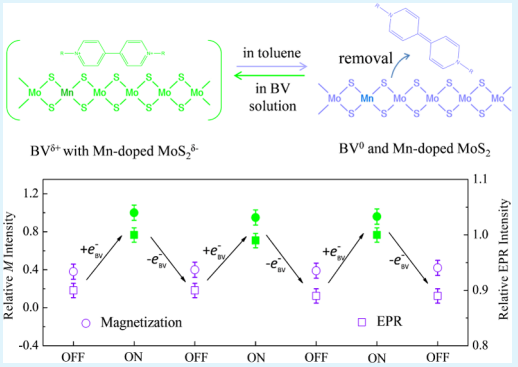

KEYWORDS: *2D van der Waals crystals, interface charge transfer, reversible manipulation, magnetic interaction, first-principles calculations*

INTRODUCTION

Two dimensional (2D) van der Waals crystals with long-range ferromagnetic ordering have attracted recent attention because the combination of magnetic properties with their outstanding mechanical, electronic, and optical properties could lead to innovative magnetoelectric and magneto-optic applications.[1,2] Furthermore, reversible tuning of magnetic properties at room temperature in these 2D materials will be helpful for the development of spintronics, logic and memory operations, and other quantum information devices.[3−5] By means of reversible transformation of the high and low magnetic states, information storage and processing can be realized (high and low states correspond to "1" and "0" states, respectively). Toward this goal, different experimental approaches have been attempted to tune the magnetism of 2D materials, such as changing the dopant concentrations,[6,7] forming heterostructures,[8] adsorbing hydrogen at the surface,[9,10] doping Li^+ ions,[11] and so on. However, these approaches have limited practical applications in spin-based technologies since they are single way in altering the magnetic properties. New approaches to render 2D materials with stable, reversible magnetism are to be further developed.

Robust long-range room-temperature ferromagnetism has been activated on MoS_2 nanosheets, a typical 2D material, by using strategies of inducing defects or doping alien magnetic ions, which have been widely applied in traditional diluted magnetic semiconductors.[12−15] However, the ferromagnetism of an MoS_2 system induced by defects such as vacancy, strain, or zigzag edges is unstable and could hardly be controlled or manipulated by external fields as achieved in colloidal Mn-doped ZnO nanocrystals.[16] Efforts are still underway to develop air-stable MoS_2-based materials for reversible tuning of the ferromagnetism. Fortunately, Mn-doped MoS_2 nanosheets have been demonstrated as air-stable materials with long-range intrinsic ferromagnetic ordering and offer an excellent platform for magnetism transformation.[17,18] Inspired by a number of studies showing the flexible tuning of electronic structures of 2D materials by molecular adsorption,[19,20] the magnetic behavior of Mn-doped MoS_2 nanosheets might also be tuned by molecular adsorption since their magnetism is intimately related to their electronic structures. Among a

Received: July 11, 2018
Accepted: August 29, 2018
Published: August 29, 2018

DOI: 10.1021/acsami.8b11623
ACS Appl. Mater. Interfaces 2018, 10, 31648−31654

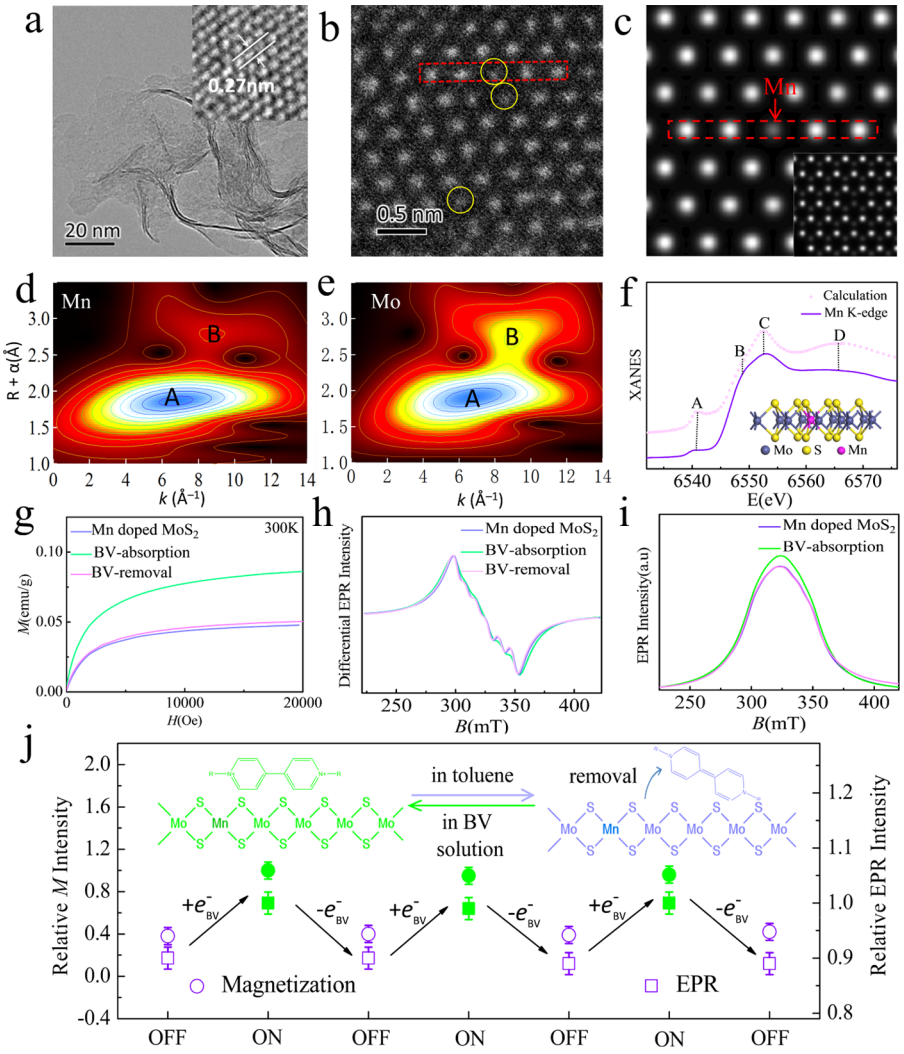

Figure 1. (a) TEM and HRTEM images, (b) HAADF-STEM image, and (c) the simulated image of Mn-doped MoS_2 nanosheets. Wavelet transforms for the k^3-weighted EXAFS signals at Mn (d) and Mo (e) K-edges for Mn-doped MoS_2 nanosheets. (f) Experimental and calculated Mn K-edge XANES spectra of the Mn-doped MoS_2 nanosheets: the inset is the model structure of Mn occupation sites in the MoS_2 lattice. (g) Magnetization vs magnetic field ($M-H$) curves at 300 K, (h) absorption-mode electron paramagnetic resonance (EPR) spectra, and (i) derivative-mode EPR spectra. (j) The reversibility of the magnetism and EPR signal changes in Mn-doped MoS_2 nanosheets upon adsorption/desorption of BV molecules: the inset is the schematic representation of the adsorption/desorption of BV molecules (the phenyl rings are represented by R for simplification) on the surface of Mn-doped MoS_2 nanosheets.

diversity of electron-donating organic molecules, benzyl viologen (BV) is considered as a reasonable choice. The charge injected into the Mn-doped MoS_2 nanosheets could help to control magnetic states in Mn-doped MoS_2 nanosheets by tuning the band gap structure because of its lowest reduction potentials.[21−23] In addition, the adsorbed BV molecules can be easily removed by immersion in toluene. As such, an adsorption/desorption process does not induce phase transition or destroy the pristine MoS_2 structure, and it possesses the ability to reversibly tune the magnetic states of Mn-doped MoS_2 nanosheets through selective removal of surface dopants. More importantly, during the adsorption/desorption process, the injection/removal of electrons is analogous to electrical control in spintronics devices, suggesting the possibility of tuning the magnetism of transition-metal-doped MoS_2 nanosheets by using an external electrical field to modify the charge concentration.

In this work, we demonstrate an effective way of reversibly tuning ferromagnetic behaviors of Mn-doped MoS_2 nanosheets by using BV molecules as a charge donor. The saturation magnetic moment of the nanosheets increases from 0.05 to 0.08 emu/g upon BV adsorption and then reversibly returns to 0.05 emu/g after BV desorption. A combination of detailed experimental characterizations and first-principles calculations clarifies that in the BV-adsorbed MoS_2 nanosheets, the electrons donated by BV molecules increase the magnetic moment of Mn atoms and enlarge the radii of the bound magnetic polaron (BMP), thus giving rise to enhanced ferromagnetism.

RESULTS AND DISCUSSION

The Mn-doped MoS_2 nanosheets were obtained by a supercritical hydrothermal reaction (Figure S1). The morphology of the obtained products can be directly observed by the transmission electron microscopy (TEM) image in Figure 1a. A faint contrast verifies the ultrathin nature of the nanosheets, and the high-resolution TEM (HRTEM) image in the inset shows the hexagonal structure of MoS_2 with a fringe spacing of

DOI: 10.1021/acsami.8b11623
ACS Appl. Mater. Interfaces 2018, 10, 31648−31654

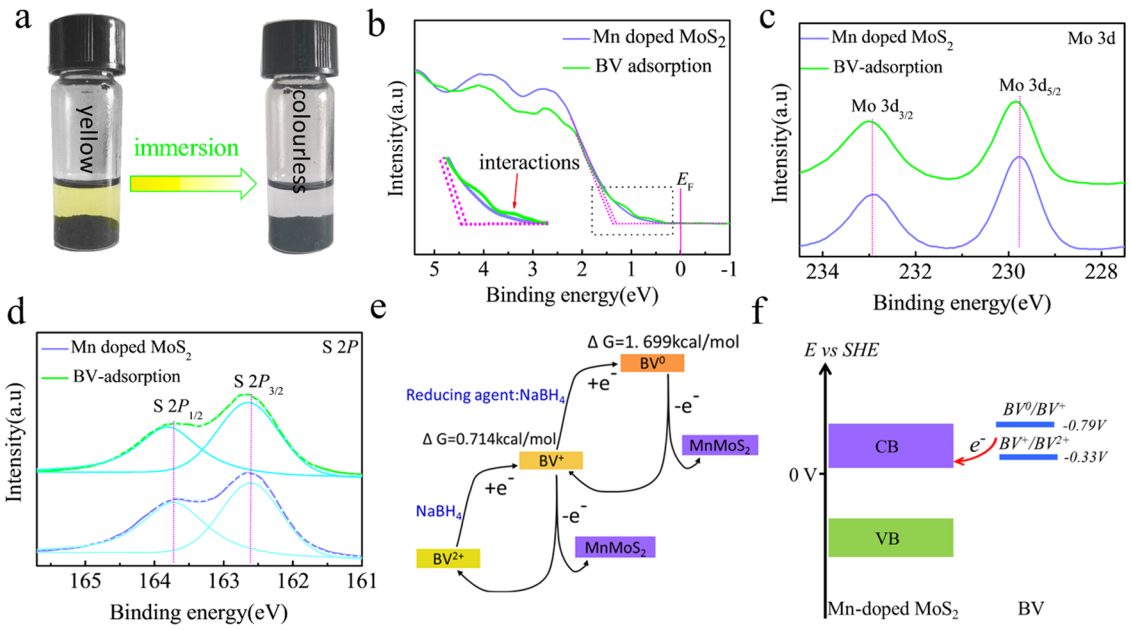

Figure 2. (a) Color change from yellow to colorless of the BV solution after immersion of Mn-doped MoS_2 nanosheets; (b) UPS spectra; and (c) Mo 3d and (d) S 2p XPS spectra of Mn-doped MoS_2 nanosheets with/without adsorption of the BV molecules. (e) Reversible redox reaction with Gibbs free-energy difference. (f) Energy band diagram of Mn-doped MoS_2 and BV redox states.

~0.27 nm corresponding to the (100) planes. The cross-sectional TEM image (Figure S2) reveals that these nanosheets mainly contain one to five atomic layers with a layer spacing of 0.63 nm. The substitutional doping of Mn (marked by yellow circles in Figure 1b) is convincingly evidenced by detailed characterizations, including high-angle annular dark-field scanning transmission electron microscopy (HAADF-STEM) and X-ray absorption fine structure (XAFS) spectra. We simulated the HAADF image for the Mn-substituted configuration, as shown in Figure 1c, which is in agreement with the experimental image (Figure 1b), as supported by the intensity line profiles in Figure S4. The Mn substitution is further confirmed by detailed analysis of extended X-ray absorption fine structure (EXAFS) analysis at the Mn K-edge (Figure S5). The wavelet transfer (WT) of the Mn K-edge EXAFS data shows that there are two maxima (marked as A and B) at the cross-point of R_A = 1.9 Å/k_A = 6.8 Å^{-1} and R_B = 2.9 Å/k_B = 8.7 Å^{-1} (Figure 1d), just like that for the Mo K-edge (Figure 1e) WT map. This implies the presence of S and Mo neighbors surrounding Mn atoms, respectively, and affords direct evidence for the substitution of Mn for the Mo sites in MoS_2. The main spectral features of the Mn K-edge XANES experimental spectrum could be reproduced by XANES calculation using FEFF8.2 code for the model of Mn-doped MoS_2, which also confirms the substitutional nature of Mn atoms (Figure 1f). The X-ray photoelectron spectroscopy (XPS) spectra shown in Figure S6 indicates the 2+ valence of Mn dopants, in agreement with the theoretical calculations later (see the Supporting Information for a detailed analysis). Besides, the inductively coupled plasma analysis reveals that the atomic ratio of Mn/Mo is ~3.0:97.0. All of these results indicate the successful synthesis of Mn-doped MoS_2 nanosheets by the supercritical hydrothermal method.

To tune the magnetic behavior of Mn-doped MoS_2 nanosheets, the neutral BV molecule (BV^0) was used as the surface charge-transfer donor. The reduction procedure of BV is shown in Figure S7. We tested BV^0 solutions with various concentrations (Figure S8) and chose the 10 mM solution shown in Figure 1g as a typical case to study the role of BV in tuning the magnetism (analysis details are given in Figure S8). As seen in Figure S9, the pristine Mn−MoS_2 nanosheets exhibit ferromagnetic behavior at room temperature because of the well-defined hysteresis loop with a coercivity of 45 Oe, a remnant magnetism of 0.001 emu/g, and a saturation magnetization of 0.05 emu/g. The field-cooling and zero-field-cooling curves (Figure S9b) suggest that the Curie temperature (T_C) of the Mn-doped MoS_2 nanosheets is above 350 K. With the adsorption/removal of BV molecules, the coercivity and saturation magnetization of the Mn−MoS_2 nanosheets show reversible changes. For instance, the adsorption of BV^0 molecules could significantly increase the saturation magnetic moment of Mn-doped MoS_2 nanosheets from ~0.05 to ~0.08 emu/g; after removal of the BV molecules by immersing the nanosheets in toluene, the saturation magnetic moment restores its original value of ~0.05 emu/g. Notably, the BV adsorption/desorption did not change the pristine structure of the Mn-doped MoS_2 nanosheets as indicated by the X-ray diffraction patterns in Figure S10. From the electron paramagnetic resonance (EPR) spectra of the BV-adsorbed nanosheets, the typical hyperfine structure with six lines arising from the interaction of Mn electron spin with its nuclear spin of I = 5/2 is broadened considerably (Figure 1h) and the EPR signal in the derivative mode (Figure 1i) is intensified compared to the BV-free nanosheets. Such a change is caused by the interactions between the substitutional Mn atoms and the alien electrons induced by the BV molecule. We compare the change of saturation magnetic moment and the EPR signal in Mn-doped MoS_2 nanosheets in Figure 1j. The ferromagnetic behavior in Mn-doped MoS_2 nanosheets could be reversibly tuned through the adsorption/desorption process of BV molecules as schematically shown in the inset of Figure 1j. During three cycles of adsorption/desorption of BV molecules, the intensity of the magnetism in BV-adsorbed Mn-doped MoS_2 nanosheets

DOI: 10.1021/acsami.8b11623
ACS Appl. Mater. Interfaces 2018, 10, 31648−31654

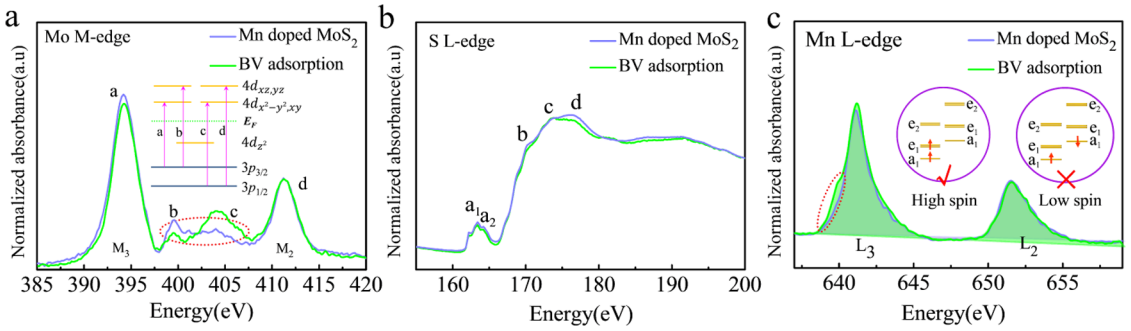

Figure 3. (a) Mo M-edge, (b) S L-edge, and (c) Mn L-edge XANES spectra of Mn-doped MoS_2 with/without adsorption of the BV molecules.

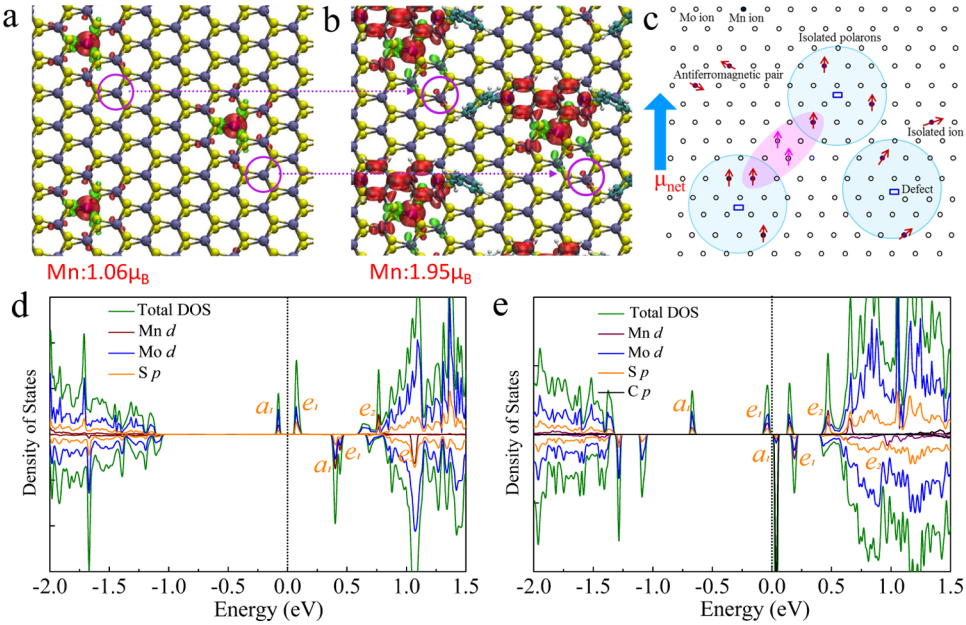

Figure 4. Spin density ($\rho\uparrow - \rho\downarrow$) for Mn-doped MoS_2 nanosheets without (a) and with (b) adsorption of the BV molecules. Red and aqua isosurfaces represent positive and negative spin densities, respectively. (c) Schematic presentation of magnetic polarons. Calculated DOS for Mn-doped MoS_2 nanosheets without (d) and with (e) adsorption of BV molecules.

is 60% more intense than that of the nonadsorbed sample; after removing the BV molecules, the original saturation magnetic moment is restored. This reversible process can be repeated 20 times on the same sample without detectable degradation (Figure S11). It can also be seen that the EPR signal can well track the saturation magnetic moment. A similar phenomenon has been observed by Ochsenbein et al. on Mn-doped ZnO, where the injected electrons lead to a synchronous increase of the saturation magnetic moment with the EPR signal intensity.[16] This leads us to believe that the reversibly changed magnetic property of Mn-doped MoS_2 nanosheets is intimately correlated with the BV molecules adsorbed on the Mn-doped MoS_2 nanosheets.

Figure 2a shows the color change, from yellowish to colorless, of the BV solution after immersing the Mn-doped MoS_2 nanosheets into it. The color change suggests that the yellowish BV^0 molecules are effectively adsorbed on the surface of Mn-doped MoS_2 nanosheets. Consequently, the ultraviolet photoelectron spectroscopy (UPS) spectra in Figure 2b display two new characteristic shoulder peaks near the valence band maximum (VBM). At the same time, the VBM shifts from 1.30 eV below the Fermi level (E_F) to 1.37 eV below E_F. This is indicative of the electron interaction between the BV molecules and the Mn-doped MoS_2 nanosheets, with nontrivial electron transfer from BV molecules to Mn-doped MoS_2 nanosheets. The XPS spectra of Mo 3d (Figure 2c) and S 2p (Figure 2d) show a uniform shift toward a higher binding energy after BV adsorption, suggesting the n-type doping of BV molecules, in line with the published XPS results.[24−27] More evidence of the electron transfer from BV to Mn-doped MoS_2 nanosheets could be found from the Raman spectra (Figure S12). For Mn-doped MoS_2 nanosheets, the Raman spectrum displays an A_{1g} peak that is slightly blue-shifted after BV adsorption,[28] suggesting the change of electronic structure of Mn-doped MoS_2 caused by the charge transfer. The charge transfer involves a two-electron redox reaction ($BV^0 \rightarrow BV^+ \rightarrow BV^{2+}$, Figure 2e). As depicted in the energy diagram, BV molecules have a relatively lower reduction potential than the Mn-doped MoS_2 (Figure 2f), e.g., about −0.33 V (BV^+/BV^{2+}) and −0.79 V (BV^0/BV^+) vs the standard hydrogen electrode (SHE),[29] while the position of the conduction band edge of the Mn-doped MoS_2 is located near 0 V vs SHE.[17,30] Due to the energy-level offset, the neutral BV molecule (BV^0) acting as an effective electron donor can readily donate electrons to the conduction band of Mn-doped MoS_2 nanosheets and then they reach the BV^{2+} state. More importantly, the difference of Gibbs

DOI: 10.1021/acsami.8b11623
ACS Appl. Mater. Interfaces 2018, 10, 31648−31654

free energy between BV^{2+} and BV^0 is as large as 2.4 kcal/mol (Figure 2e); this explains the air stability of the BV-adsorbed Mn-doped MoS_2 because it prevents the reduction of BV^{2+} to BV^0 under ambient conditions.

To understand the changes of electronic structures upon electron transfer from BV to Mn-doped MoS_2 nanosheets, in Figure 3a,c, we show the XANES spectra, which are element-specific and reflect mainly the electronic features of the unoccupied states. The Mo $M_{2,3}$-edge XANES spectra of Mn-doped MoS_2 nanosheets exhibits four characteristic peaks of a, b, c, and d. The peaks a and b correspond to the electron transition from Mo $3p_{3/2}$ to unoccupied $4d_{x^2-y^2,xy}$ and $4d_{xz,yz}$ orbitals, while the peaks c and d arise from the transition from Mo $3p_{1/2}$ to the $4d_{x^2-y^2,xy}$ and $4d_{xz,yz}$ orbitals, respectively. After adsorption of BV molecules, quite different changes of these peaks are observed: the peak intensities of a and b decrease, the intensity of d remains almost unchanged, while the intensity of c increases. This implies that the electrons in Mo 4d levels are redistributed after the electron transfer from BV to Mn-doped MoS_2 nanosheets. In contrast to the Mo $M_{2,3}$-edge spectra, the S $L_{2,3}$-edge XANES spectra in Figure 3b only show a slight intensity decrease of peak d, which is attributed to S 2p electron transition to empty S 3d-like states,[31] suggesting increased electron occupation of S. Similar changes to the Mo $M_{2,3}$-edge XANES spectra are also observed on the Mn $L_{2,3}$-edge spectra caused by BV adsorption. A new shoulder peak appears on the lower energy side of the L_3 peak, suggesting the reduced valence of substitutional Mn after BV adsorption. That is, more electrons occupy the Mn 3d states. According to the branching intensity ratio of $I(L_3)/[I(L_3) + I(L_2)] = 0.67$,[32] we deduce that the Mn atoms are in a high-spin state when BV is adsorbed. In other words, the electrons transferred from BV occupy the spin-up Mn 3d e_1 orbitals, rather than the spin-down a_1 orbitals, as illustrated in the inset of Figure 3c. These spectroscopic results reinforce our above conclusion that the alien electrons brought by BV molecules play critical roles in mediating the ferromagnetism of Mn-doped MoS_2 nanosheets.

Taking together, the ferromagnetic response of Mn-doped MoS_2 nanosheets could be switched reversibly through the adsorption/desorption of BV molecules. As an electron donor, the adsorption position of the BV molecule is on a pristine MoS_2 monolayer along the diagonal of the unit cell, as shown in Figure S13.[33] On the basis of this structure model, we employed the ABINIT software package to calculate the electronic structures of the Mn-doped MoS_2 with/without BV adsorption. The calculation details are included in the Supporting Information. The obtained spin density and density of states (DOSs) are shown in Figure 4a,b and 4d,e, respectively. For the Mn-doped MoS_2 nanosheets, the Mn 3d orbitals are split into two 2-fold-degenerate e_1 (d_{xz/x^2-y^2}) and e_2 ($d_{xz/yz}$) states and a fully occupied a_1 (d_{z^2}) state under the C_{3v} symmetry,[34] in agreement with previous calculations.[34,35] When the BV molecules are adsorbed on the surface of Mn-doped MoS_2 nanosheets, besides the occupied a_1 orbitals, the spin-up e_1 orbitals are also occupied. The Bader charge analysis further shows that, on average, about 1.07*e* electron is transferred from BV molecules to the Mn-doped MoS_2 monolayer. In other words, BV adsorption causes the high-spin electronic configuration of substitutional Mn, in line with the Mn $L_{2,3}$-edge XANES results. Accompanied with the BV adsorption, the magnetic moment increases from 1.06 to 1.95 μ_B/Mn, as indicated in Figure 4a,b. The second-nearest neighboring Mo (marked by purple circles) of Mn couples ferromagnetically to the Mn atom after BV adsorption, consistent with the Mo $M_{2,3}$-edge XANES spectra (Figure 3a), which indicate the redistribution of Mo 4d electrons as mentioned above. Considering the low content (≈3 atom %) of Mn in the MoS_2 nanosheets, the bound magnetic polaron (BMP) model, as shown in Figure 4c, is suitable to interpret the origins of ferromagnetism and the enhanced magnetic moment. Within the framework of BMP, the increase of Mn saturation magnetic moment could intensify the macroscopic magnetism of the Mn-doped MoS_2 nanosheets. Besides, the magnetic interactions between Mn atoms and distant Mo atoms due to the spin polarization could enlarge the effective radii of the bound magnetic polarons, benefiting the macroscopic magnetism of Mn-doped MoS_2 nanosheets. The synergetic effect of the increased magnetic moment of Mn atoms and the spin polarization of distant Mo atoms make the magnetic moment in Mn-doped MoS_2 nanosheets increase from ∼0.05 to ∼0.08 emu/g, as experimentally observed. After removing BV molecules, the magnetic moment is restored. Remarkably, only a small portion of the Mn ions are contained in the overlapped polarons; this is the reason why the observed saturation magnetic moment of the Mn^{2+} ions is far smaller than the theoretical value. Hence, taking into account the experimental and theoretical results, we may draw the conclusion that the reversible process of introducing/depleting electrons via adsorption/desorption of BV molecules is the underlying reason for tuning the magnetic behavior of the Mn-doped MoS_2 nanosheets.

CONCLUSIONS

In summary, we have successfully doped Mn ions into MoS_2 nanosheets and obtained ferromagnetism at room temperature with a magnetic moment of 0.05 emu/g. More interestingly, the ferromagnetism in the as-synthesized nanosheets could be reversibly tuned by interface charge transfer through adsorption/desorption of BV molecules. On the basis of experimental characterizations and first-principles calculations, the reversible process of introducing/depleting electrons through adsorption/desorption of BV molecules is responsible for the tuning of the magnetic behavior of the Mn-doped MoS_2 nanosheets. This work shows that interface charge transfer could provide an effective pathway for manipulation of the magnetic behavior of two-dimensional magnetic semiconductor materials.

EXPERIMENTAL SECTION

Synthesis of Mn-Doped MoS_2 Nanosheets. Typically, 0.9 g of $(NH_4)_6Mo_7O_{24}\cdot 4H_2O$ (Sigma-Aldrich) and 0.085 g of Mn-$(CH_3COO)_2\cdot 4H_2O$ (Sigma-Aldrich) were dissolved in 20 mL of deionized water. After ultrasonication for 30 min to form a homogeneous solution, 10 mL of CS_2 was added into the solution and transferred into a stainless steel autoclave under Ar atmosphere, which was then sealed and maintained at 400 °C for 1 h. Then, the autoclave was allowed to cool down naturally. The produced black precipitates were centrifugated and treated with saturated NaOH solution for 3 h and then washed with ethanol and water three times, respectively. The final products were dried at 60 °C under vacuum.

Synthesis of BV Molecule. Briefly, 0.05 mmol benzyl viologen dichloride (Sigma-Aldrich) was dissolved in 5 mL of deionized water and 5 mL of toluene was added to form a bilayer solution. Then, 3.7 g of sodium borohydride (Sigma-Aldrich) was added to the water/toluene bilayer solution, and 1 day after the reaction, the top toluene layer was extracted for use.

DOI: 10.1021/acsami.8b11623
ACS Appl. Mater. Interfaces 2018, 10, 31648−31654

BV Adsorption/Desorption. Briefly, 0.1 g of Mn-doped MoS_2 nanosheets was immersed in the BV solution for 48 h. After that, the products were collected by centrifugation and dried under vacuum at 50 °C to remove the excess molecule and solvent and obtain BV-adsorbed Mn-doped MoS_2 nanosheets. To remove the BV molecule from the Mn−MoS_2 nanosheets, the as-prepared sample was ultrasonically cleaned in toluene five times. Then, the obtained products were collected by centrifugation and dried at 50 °C under vacuum.

■ ASSOCIATED CONTENT

Supporting Information

The Supporting Information is available free of charge on the ACS Publications website at DOI: 10.1021/acsami.8b11623.

Experimental details, TEM images, X-ray diffraction pattern, EPR spectra, XANES spectra, and density functional theory calculation details and analysis (PDF)

■ AUTHOR INFORMATION

Corresponding Authors

*E-mail: zhsun@ustc.edu.cn (Z.S.).
*E-mail: ywsh2000@ustc.edu.cn (W.Y.).

ORCID

Zhihu Sun: 0000-0002-3898-969X
Wensheng Yan: 0000-0001-6297-4589

Notes

The authors declare no competing financial interest.

■ ACKNOWLEDGMENTS

This work was supported by the National Natural Science Foundation of China (Grant Nos. 11435012, U1632263, 21533007, 11775225, and 11604341) and the Foundation for Innovative Research Groups of the National Natural Science Foundation of China (11621063). The authors acknowledge BSRF, SSRF, and NSRL for the synchrotron beamtime.

■ REFERENCES

(1) Gong, C.; Li, L.; Li, Z.; Ji, H.; Stern, A.; Xia, Y.; Cao, T.; Bao, W.; Wang, C.; Wang, Y.; Qiu, Z. Q.; Cava, R. J.; Louie, S. G.; Xia, J.; Zhang, X. Discovery of Intrinsic Ferromagnetism in Two-Dimensional van der Waals Crystals. *Nature* **2017**, *546*, 265−269.

(2) Huang, B.; Clark, G.; Navarro-Moratalla, E.; Klein, D. R.; Cheng, R.; Seyler, K. L.; Zhong, D.; Schmidgall, E.; McGuire, M. A.; Cobden, D. H.; Yao, W.; Xiao, D.; Jarillo-Herrero, P.; Xu, X. D. Layer-Dependent Ferromagnetism in a van der Waals Crystal Down to the Monolayer Limit. *Nature* **2017**, *546*, 270−273.

(3) Pan, J.; Lany, S.; Qi, Y. Computationally Driven Two-Dimensional Materials Design: What Is Next? *ACS Nano* **2017**, *11*, 7560−7564.

(4) Kumar, H.; Frey, N. C.; Dong, L.; Anasori, B.; Gogotsi, Y.; Shenoy, V. B. Tunable Magnetism and Transport Properties in Nitride MXenes. *ACS Nano* **2017**, *11*, 7648−7655.

(5) Radisavljevic, B.; Whitwick, M. B.; Kis, A. Integrated Circuits and Logic Operations Based on Single-Layer MoS_2. *ACS Nano* **2011**, *5*, 9934−9938.

(6) Wang, T.; Li, J.; Jin, H.; Wei, Y. Tuning the Electronic and Magnetic Properties of InSe Nanosheets by Transition Metal Doping. *Phys. Chem. Chem. Phys.* **2018**, *20*, 7532−7537.

(7) Andriotis, A. N.; Menon, M. Tunable Magnetic Properties of Transition Metal Doped MoS_2. *Phys. Rev. B* **2014**, *90*, No. 125304.

(8) Tian, X. Q.; Wang, X. R.; Wei, Y. D.; Liu, L.; Gong, Z. R.; Gu, J.; Du, Y.; Yakobson, B. I. Highly Tunable Electronic Structures of Phosphorene/Carbon Nanotube Heterostructures through External Electric Field and Atomic Intercalation. *Nano Lett.* **2017**, *17*, 7995−8004.

(9) Sanchez, N.; Gallego, S.; Cerdá, J.; Muñoz, M. C. Tuning Surface Metallicity and Ferromagnetism by Hydrogen Adsorption at the Polar ZnO(0001) Surface. *Phys. Rev. B* **2010**, *81*, No. 115301.

(10) Yang, S.; Li, W.; Ye, C.; Wang, G.; Tian, H.; Zhu, C.; He, P.; Ding, G.; Xie, X.; Liu, Y.; Lifshitz, Y.; Lee, S. T.; Kang, Z.; Jiang, M. C_3N-A2D Crystalline, Hole-Free, Tunable-Narrow-Bandgap Semiconductor with Ferromagnetic Properties. *Adv. Mater.* **2017**, *29*, No. 1605625.

(11) Yan, W.; Sun, Z.; Li, Z.; Liu, Q.; Yao, T.; Pan, Z.; Wang, C.; Hu, F.; Jiang, Y.; Qi, Z.; Zeng, F.; Wei, S. Valence State-Dependent Ferromagnetism in Mn-Doped NiO Thin Films. *Adv. Mater.* **2012**, *24*, 353−237.

(12) Zhang, B. Y.; Yao, B.; Li, Y. F.; Liu, A. M.; Zhang, Z. Z.; Li, B. H.; Xing, G. Z.; Wu, T.; Qin, X. B.; Zhao, D. X.; Shan, C. X.; Shen, D. Z. Evidence of Cation Vacancy Induced Room Temperature Ferromagnetism in Li-N Codoped ZnO Thin Films. *Appl. Phys. Lett.* **2011**, *99*, No. 182503.

(13) Xing, G. Z.; Wang, D. D.; Cheng, C. J.; He, M.; Li, S.; Wu, T. Emergent Ferromagnetism in ZnO/Al_2O_3 Core-Shell Nanowires: Towards Oxide Spinterfaces. *Appl. Phys. Lett.* **2013**, *103*, No. 022402.

(14) Chen, T.; Liu, W.; Zheng, F.; Gao, M.; Pan, X.; van der Laan, G.; Wang, X.; Zhang, Q.; Song, F.; Wang, B.; Wang, B.; Xu, Y.; Wang, G.; Zhang, R. High-Mobility Sm-Doped Bi_2Se_3 Ferromagnetic Topological Insulators and Robust Exchange Coupling. *Adv. Mater.* **2015**, *27*, 4823−4829.

(15) Wang, X. F.; Xu, J. B.; Zhang, B.; Yu, H. G.; Wang, J.; Zhang, X.; Yu, J. G.; Li, Q. Signature of Intrinsic High-Temperature Ferromagnetism in Cobalt-Doped Zinc Oxide Nanocrystals. *Adv. Mater.* **2006**, *18*, 2476−2480.

(16) Ochsenbein, S. T.; Feng, Y.; Whitaker, K. M.; Badaeva, E.; Liu, W. K.; Li, X.; Gamelin, D. R. Charge-Controlled Magnetism in Colloidal Doped Semiconductor Nanocrystals. *Nat. Nanotechnol.* **2009**, *4*, 681−687.

(17) Mishra, R.; Zhou, W.; Pennycook, S. J.; Pantelides, S. T.; Idrobo, J.-C. Long-Range Ferromagnetic Ordering in Manganese-Doped Two-Dimensional Dichalcogenides. *Phys. Rev. B* **2013**, *88*, No. 144409.

(18) Tan, H.; Hu, W.; Wang, C.; Ma, C.; Duan, H.; Yan, W.; Cai, L.; Guo, P.; Sun, Z.; Liu, Q.; et al. Intrinsic Ferromagnetism in Mn - Substituted MoS_2 Nanosheets Achieved by Supercritical Hydrothermal Reaction. *Small* **2017**, *13*, No. 1701389.

(19) Liu, Y.; Xu, F.; Zhang, Z.; Penev, E. S.; Yakobson, B. I. Two-Dimensional Mono-Elemental Semiconductor with Electronically Inactive Defects: The Case of Phosphorus. *Nano Lett.* **2014**, *14*, 6782−6786.

(20) Yu, Z.; Pan, Y.; Shen, Y.; Wang, Z.; Ong, Z.-Y.; Xu, T.; Xin, R.; Pan, L.; Wang, B.; Sun, L. Towards Intrinsic Charge Transport in Monolayer Molybdenum Disulfide by Defect and Interface Engineering. *Nat. Commun.* **2014**, *5*, No. 5290.

(21) Yu, W. J.; Liao, L.; Chae, S. H.; Lee, Y. H.; Duan, X. Toward Tunable Band Gap and Tunable Dirac Point in Bilayer Graphene with Molecular Doping. *Nano Lett.* **2011**, *11*, 4759−4763.

(22) Kiriya, D.; Tosun, M.; Zhao, P.; Kang, J. S.; Javey, A. Air-Stable Surface Charge Transfer Doping of MoS_2 by Benzyl Viologen. *J. Am. Chem. Soc.* **2014**, *136*, 7853−7856.

(23) Montalti, M.; Credi, A.; Prodi, L.; Gandolfi, M. T. *Handbook Of Photochemistry*; CRC press, 2006.

(24) Lin, J. D.; Han, C.; Wang, F.; Wang, R.; Xiang, D.; Qin, S.; Zhang, X.-A.; Wang, L.; Zhang, H.; Wee, A. T. S.; Chen, W. Electron-Doping Enhanced Trion Formation in Monolayer Molybdenum Disulfide Functionalized with Cesium Carbonate. *ACS Nano* **2014**, *8*, 5323−5329.

(25) Fang, H.; Tosun, M.; Seol, G.; Chang, T. C.; Takei, K.; Guo, J.; Javey, A. Degenerate n-Doping of Few-Layer Transition Metal Dichalcogenides by Potassium. *Nano Lett.* **2013**, *13*, 1991−1995.

(26) Kaushik, N.; Karmakar, D.; Nipane, A.; Karande, S.; Lodha, S. Interfacial n-Doping Using an Ultrathin TiO_2 Layer for Contact

DOI: 10.1021/acsami.8b11623
ACS Appl. Mater. Interfaces 2018, 10, 31648−31654

Resistance Reduction in MoS_2. *ACS Appl. Mater. Interfaces* **2016**, *8*, 256−263.
(27) Coy Diaz, H.; Addou, R.; Batzill, M. Interface Properties of CVD Grown Graphene Transferred onto $MoS_2(0001)$. *Nanoscale* **2014**, *6*, 1071−1078.
(28) Suh, J.; Park, T. E.; Lin, D. Y.; Fu, D.; Park, J.; Jung, H. J.; Chen, Y.; Ko, C.; Jang, C.; Sun, Y.; Sinclair, R.; Chang, J.; Tongay, S.; Wu, J. Doping Against the Native Propensity of MoS_2: Degenerate Hole Doping by Cation Substitution. *Nano Lett.* **2014**, *14*, 6976−6982.
(29) Kim, S. M.; Jang, J. H.; Kim, K. K.; Park, H. K.; Bae, J. J.; Yu, W. J.; Lee, I. H.; Kim, G.; Dinh Loc, D.; Kim, U. J.; Lee, E.-H.; Shin, H.-J.; Choi, J.-Y.; Lee, Y. H. Reduction-Controlled Viologen in Bisolvent as an Environmentally Stable n-Type Dopant for Carbon Nanotubes. *J. Am. Chem. Soc.* **2009**, *131*, 327−331.
(30) Fontana, M.; Deppe, T.; Boyd, A. K.; Rinzan, M.; Liu, A. Y.; Paranjape, M.; Barbara, P. Electron-Hole Transport and Photovoltaic Effect in Gated MoS_2 Schottky Junctions. *Sci. Rep.* **2013**, *3*, No. 1634.
(31) Li, D.; Bancroft, G.; Kasrai, M.; Fleet, M.; Feng, X.; Tan, K. Polarized X-Ray Absorption Spectra and Electronic Structure of Molybdenite $(2H\text{-}MoS_2)$. *Phys. Chem. Miner.* **1995**, *22*, 123−128.
(32) Thole, B. T.; Van der Laan, G. Branching Ratio in X-Ray Absorption Spectroscopy. *Phys. Rev. B* **1988**, *38*, 3158.
(33) Jing, Y.; Tan, X.; Zhou, Z.; Shen, P. Tuning Electronic and Optical Properties of MoS_2 Monolayer via Molecular Charge Transfer. *J. Mater. Chem. A* **2014**, *2*, 16892−16897.
(34) Cheng, Y. C.; Zhu, Z. Y.; Mi, W. B.; Guo, Z. B.; Schwingenschlögl, U. Prediction of Two-Dimensional Diluted Magnetic Semiconductors: Doped Monolayer MoS_2 Systems. *Phys. Rev. B* **2013**, *87*, No. 100401.
(35) Ramasubramaniam, A.; Naveh, D. Mn-Doped Monolayer MoS_2: An Atomically Thin Dilute Magnetic Semiconductor. *Phys. Rev. B* **2013**, *87*, No. 195201.

DOI: 10.1021/acsami.8b11623
ACS Appl. Mater. Interfaces 2018, 10, 31648−31654